Probing the all-ferrous states of methanogen nitrogenase iron proteins

Joseph B. Solomon,[†,‡,‖] Mahtab F. Rasekh,[†,‡,‖] Caleb J. Hiller,[§,‖] Chi Chung Lee,[†] Kazuki Tanifuji,[†] Markus W. Ribbe,[†,‡,*] Yilin Hu[†,*]

[†]Department of Molecular Biology and Biochemistry, University of California, Irvine, CA92697-3900

[‡]Department of Chemistry, University of California, Irvine, CA 92697-2025

[§]Department of Physical Science, Southern Utah University, Cedar City, UT 84720

ABSTRACT: The Fe protein of nitrogenase reduces two C1 substrates, CO_2 and CO, under ambient conditions when its $[Fe_4S_4]$ cluster adopts the all-ferrous $[Fe_4S_4]^0$ state. Here we show disparate reactivities of the *nifH*- and *vnf*-encoded Fe proteins from *Methanosarcina acetivorans* (designated *Ma*NifH and *Ma*VnfH) towards C1 substrates in the all-ferrous state, with the former capable of reducing both CO_2 and CO to hydrocarbons, and the latter only capable of reducing CO to hydrocarbons at substantially reduced yields. EPR experiments conducted at varying solution potentials reveal that *Ma*VnfH adopts the all-ferrous state at a more positive reduction potential than *Ma*NifH, which could account for the weaker reactivity of the *Ma*VnfH towards C1 substrates than *Ma*NifH. More importantly, *Ma*VnfH already displays the $g = 16.4$ parallel-mode EPR signal that is characteristic of the all-ferrous $[Fe_4S_4]^0$ cluster at a reduction potential of –0.44 V, and the signal reaches 50% maximum intensity at a reduction potential of –0.59 V, suggesting the possibility of this Fe protein to access the all-ferrous $[Fe_4S_4]^0$ state under physiological conditions. These results bear significant relevance to the long-lasting debate of whether the Fe protein can utilize the $[Fe_4S_4]^{0/2+}$ redox couple to support a two-electron transfer during substrate turnover and, therefore, is crucial for expanding our knowledge of the reaction mechanism of nitrogenase and the cellular energetics of nitrogenase-based processes.

Keywords: nitrogenase, Fe protein, $[Fe_4S_4]$ cluster, all-ferrous state, physiological reduction potential, CO_2 reduction, hydrocarbon formation, methanogen

The iron sulfur (FeS) proteins play crucial roles in biological processes that range from iron homeostasis and gene regulation to electron transfer and enzyme catalysis.[1-5] A member of the FeS protein family, the iron (Fe) protein is the reductase component of nitrogenase, a key enzyme in the global nitrogen cycle that catalyzes the ambient reduction of the atmospheric N_2 to the bioavailable NH_3. Encoded by *nifH* and *vnfH*, respectively, the Fe proteins of Mo- and V-nitrogenases (designated NifH and VnfH) are structurally homologous homodimers that house a surface-exposed $[Fe_4S_4]$ cluster at the subunit interface and an MgATP-binding site within each subunit. During substrate turnover, NifH or VnfH forms a functional complex with its catalytic partner, NifDK or VnfDGK, which allows electrons to be transferred concomitantly with ATP hydrolysis from the $[Fe_4S_4]$ cluster of the former, via a so-called

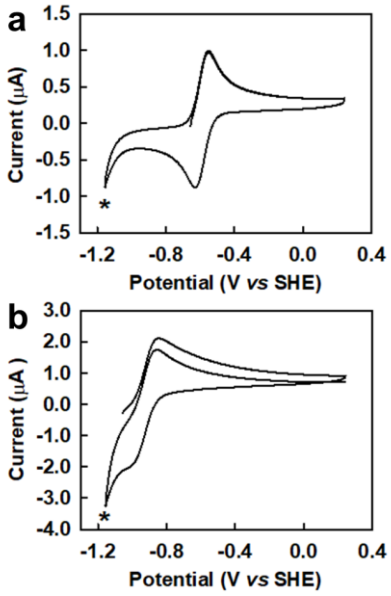

Figure 1. Cyclic voltammograms of (a) Eu(II)-DOTAM and (b) Eu(II)-DOTA in 25 mM Tris-HCl buffer at pH 8.0. The irreversible features, indicated by * at approximately –1.2 V, are attributed to the reduction of the solvent.

P- or P*-cluster, to the M- or V-cluster (generally termed the cofactor) of the latter, where substrate reduction takes place (Figure S1a).[6-8] Other than serving as an obligate electron donor for its catalytic partner in the complete nitrogenase enzyme system, the Fe protein can act as a reductase on its own and catalyze the ambient reduction of CO_2 and CO (Figure S1b).[9-11] The reactivity of Fe protein towards C1 substrates was first observed in *Azotobacter vinelandii*, a soil bacterium, where both NifH and VnfH proteins of this microorganism were shown to reduce CO_2 to CO under *in vitro* or *in vivo* conditions.[10] Subsequently, the NifH protein of a methanogenic organism, *Methanosarcina acetivorans*, was demonstrated to reduce CO_2 and CO to hydrocarbons under *in vitro* conditions.[11] These observations have established the Fe protein as a simple FeS enzyme that is capable of generating hydrocarbons via reactions that resemble the Fischer–Tropsch (FT) process[12] that is

used for the industrial production of carbon fuels; however, unlike the FT process, the reactions catalyzed by the Fe protein utilize protons/electrons (instead of H_2) as the reducing power, and they occur at ambient temperature and pressure.

The ability of the Fe protein to serve as a reductase relies on the redox versatility of its [Fe4S4] cluster, which can reversibly adopt at least three oxidation states: the super-reduced, all-ferrous state ($[Fe_4S_4]^0$), the reduced state ($[Fe_4S_4]^{1+}$) and the oxidized state ($[Fe_4S_4]^{2+}$).[1,13] The ability of the Fe protein to adopt the all-ferrous state makes it unique among the [Fe4S4]-cluster-containing proteins that are usually confined to two oxidation states other than the super-reduced state,[14] although it is unclear whether the all-ferrous state can be reached by the Fe protein under physiological conditions. Nevertheless, while it is generally believed that the $[Fe_4S_4]^{1+/2+}$ redox couple is used by the Fe protein for a one-electron transfer to its catalytic partner during nitrogenase catalysis, it has been suggested that the Fe protein could also use the $[Fe_4S_4]^{0/2+}$ couple for a two-electron transfer in this process. Likewise, the reduction of CO_2 and/or CO by the Fe protein on its own is best achieved in the presence of europium(II) diethylenetriaminepentaacetic acid [Eu(II)-DTPA] ($E_{1/2}$ = –1.14 V at pH 8),[15] a strong reductant that renders the [Fe4S4] cluster of the Fe protein in the 'super-reduced', all-ferrous $[Fe_4S_4]^0$ state. These observations have led to the question of whether the all-ferrous state of the Fe protein can be accessed at physiological reduction potentials achieved by the *in vivo* electron donors to this protein, such as ferredoxins and flavodoxins, to enable substrate reduction in the cell.

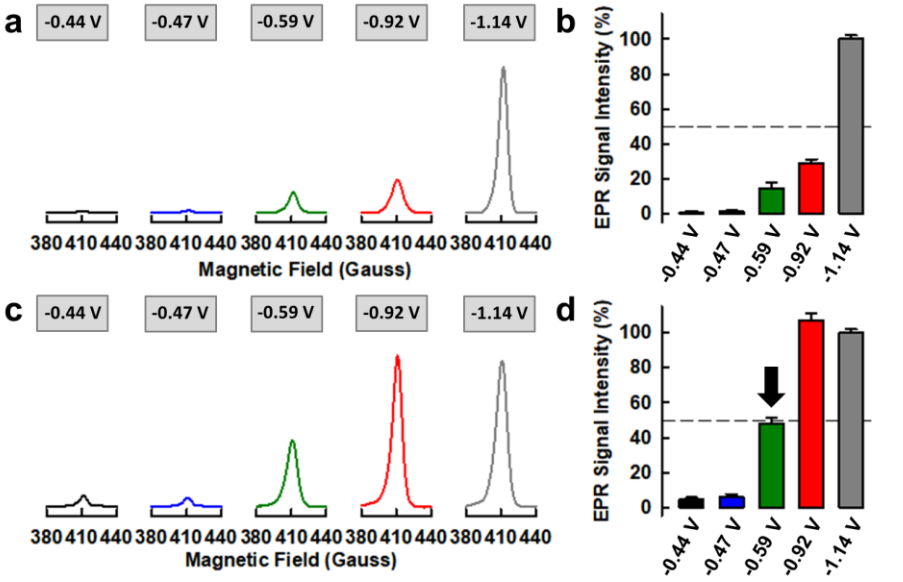

Figure 2. Titration of the all-ferrous-specific EPR signals of *Ma*VnfH and *Ma*NifH proteins *versus* solution potentials. (a, c) Appearance of the g = 16.4, parallel-mode EPR signal that is characteristic of the all-ferrous $[Fe_4S_4]^0$ cluster of *Ma*NifH (a) and *Ma*VnfH (c) in the presence of reductants with varying reduction potentials. The reductants used in this experiment were 20 mM dithionite ($E_{1/2}$ = –0.44 V at pH 8.0), 2 mM dithionite ($E_{1/2}$ = –0.47 V at pH 8.0), 10 mM Eu(II)-DOTAM ($E_{1/2}$ = –0.59 V at pH 8.0), 10 mM Eu(II)-DOTA ($E_{1/2}$ = –0.92 V at pH 8.0), and 10 mM Eu(II)-DTPA ($E_{1/2}$ = –1.14 V at pH 8.0). (b, d) The intensity of the g = 16.4 parallel-mode EPR signal *versus* the potential of the reductant used to generate the signal. The EPR signal intensity (%) was determined by double integration of the g = 16.4 signal and calculation of the relative intensity *versus* the maximum intensity at –1.14 V. The colored bars represent the EPR signal intensities (%) at $E_{1/2}$ = –0.44 V (*black*), $E_{1/2}$ = –0.47 V (*blue*), $E_{1/2}$ = –0.59 V (*green*), $E_{1/2}$ = –0.92 V (*red*) and $E_{1/2}$ = –1.14 V (*gray*). The EPR signal intensities (%) are 1.1±0.5, 1.6±0.3, 14.8±3.2, 29.1±2.2, and 100.0±2.1, respectively, for *Ma*NifH, and 4.7±1.1, 5.9±1.9, 48.0±3.2, 107.3±4.0, and 100.0±2.2, respectively, for *Ma*VnfH, at –0.44, –0.47, –0.59, –0.92, and –1.14 V. The 'mid-intensity' potential, or the potential corresponding to 50% of the maximum signal intensity, is indicated by a horizontal dashed line (b, d). For *Ma*NifH, this value is ~ –0.59 V (d, *arrow*).

To assess the all-ferrous state of the Fe protein, we first examined the utility of two Eu(II) chelates, europium(II) 1,4,7,10-tetrakis(carbamoylmethyl)-1,4,7,10-tetraazacyclododecane [Eu(II)-DOTAM] and europium(II) 1,4,7,10-tetraazacyclododecane-1,4,7,10-tetraacetic acid [Eu(II)-DOTA], as potential reductants to probe the response of the all-ferrous state to varying solution potentials. The reduction potentials of Eu(II)-DOTAM and Eu(II)-DOTA were determined by cyclic voltammetry measurements of *in situ* generated complexes in 25 mM Tris-HCl buffer at pH 8.0. The resultant voltammograms (**Figure 1**) show the reversible Eu(III)/Eu(II) couples at $E_{1/2}$ = –0.59 V (for Eu(II)-DOTAM) and –0.92 V (for Eu(II)-DOTA) *vs.* standard hydrogen electrode (SHE). These values are directly comparable with the reported potentials of Eu(II)-EGTA (–0.88 V *vs.* SHE) and Eu(II)-DTPA (–1.14 V *vs.* SHE) measured at pH 8.0.[15] The fact that the potentials of Eu(II)-DOTAM and Eu(II)-DOTA are intermediate between those of dithionite (*e.g.*, -0.47 V *vs.* SHE at 2 mM, pH 8.0)[16,17] and Eu(II)-DTPA makes them suitable candidates, together with the latter two reductants, for titrating the all-ferrous-specific EPR signal of the Fe protein *versus* solution potentials.

With proper reductants identified for the titration experiment, we treated the NifH and VnfH proteins from *M. acetivorans* (designated *Ma*NifH and *Ma*VnfH) with 20 mM dithionite ($E_{1/2}$ = –0.44 V at pH 8.0), 2 mM dithionite ($E_{1/2}$ = –0.47 V at pH 8.0), 10 mM Eu(II)-DOTAM ($E_{1/2}$ = –0.59 V at pH 8.0), 10 mM Eu(II)-DOTA ($E_{1/2}$ = –0.92 V at pH 8.0), and 10 mM Eu(II)-DTPA ($E_{1/2}$ = –1.14 V at pH 8.0) and monitored the appearance of the all-ferrous state specific, g = 16.4 parallel-mode EPR signal at the various reduction potentials generated by these reductants[13,18] Interestingly, despite sharing as high as 80% sequence homology,[19] *Ma*NifH and *Ma*VnfH display distinct patterns of changes in the magnitudes of their all-ferrous-specific EPR signals upon titration with the same set of reductants (**Figure 2**). In the case of *Ma*NifH, the g = 16.4 signal is hardly visible (1.1% of max. intensity) at –0.44 V, and it only becomes apparent (14.8% of max. intensity) at –0.59 V (**Figure 2a and b**). In contrast, *Ma*VnfH already displays a small, yet visible g = 16.4 signal (4.7% of max. intensity) at –0.44 V, and the signal (48% of max. intensity) is substantially stronger than that displayed by *Ma*NifH (14.8% of max. intensity) at –0.59 V (**Figure 2c and d**). The appearance of the g = 16.4 signal in the spectrum of the dithionite-treated *Ma*VnfH is surprising, as all Fe proteins characterized so far exist in the reduced $[Fe_4S_4]^{1+}$ state in the presence of dithionite and do not show the all-ferrous signal unless a lower potential is reached in the presence of a stronger reductant. For example, the $[Fe_4S_4]^{0/1+}$ couple of the NifH protein from *A. vinelandii* was determined to have a midpoint potential of –0.79 V.[20] In comparison, *Ma*VnfH already reaches ~50% of the maximum intensity of the g = 16.4 signal at –0.59 V (**Figure 2d**, *arrow*), and it has a hue consistent with that right before conversion into the characteristic reddish-pink color of the all-ferrous state at this potential (**Figure 3**). As such, it is likely that the cluster of this Fe protein can

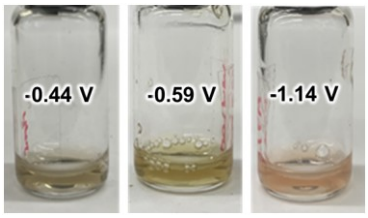

Figure 3. The *Ma*VnfH protein in 2 mM dithionite (*left*), 10 mM Eu(II)-DOTAM (*middle*), and 10 mM Eu(II)-DTPA (*right*). The $E_{1/2}$ values of the reductants are indicated.

access the all-ferrous $[Fe_4S_4]^0$ state under physiological conditions, where such a potential can be accomplished by certain ferredoxins as the electron donors to the Fe protein in the cell.[6,21-23]

The fact that *Ma*VnfH adopts the all-ferrous state at a more positive reduction potential than *Ma*NifH points to a weaker ability of *Ma*VnfH than *Ma*NifH to donate lower-potential electrons to the C1 substrates in the all-ferrous state and, consequently, a weaker ability of the all-ferrous *Ma*VnfH than its *Ma*NifH counterpart to reduce these substrates. Indeed, we observed disparate reactivities of *Ma*NifH and *Ma*VnfH toward CO_2 and CO when these assays were conducted in the presence of Eu(II)-DTPA. In the case of *Ma*NifH, both CO and hydrocarbons can be detected as products of CO_2 reduction, and the formation of CO (**Figure 4a**, *left*, *black circles*) decreases concomitantly with an increase in the formation of hydrocarbons (**Figure 4a**, *right*, *black triangles*) with increasing concentrations of Eu(II)-DTPA. The maximum yields of CO (4.55±0.19 nmol/nmol protein) and hydrocarbons (3.91±0.32 nmol/nmol protein) are accomplished by *Ma*NifH at 20 mM and 100 mM Eu(II)-DTPA, respectively. Contrary to *Ma*NifH, *Ma*VnfH shows no formation of CO (**Figure 4a**, *left*, *blue circles*) or hydrocarbons (**Figure 4a**, *right*, *blue triangles*) from CO_2 reduction under the same reaction conditions. However, like *Ma*NifH, *Ma*VnfH can generate hydrocarbons from CO reduction when Eu(II)-DTPA is supplied at 100 mM (**Figure 4b-d**). The identities of the hydrocarbon products generated by *Ma*VnfH (**Figure 4b**, *lower*), as confirmed by gas chromatograph-mass spectrometry (GC-MS) (**Figure 4d**), are the same as those generated by *Ma*NifH (**Figure 4b**, *upper*), which include C1-C4 alkanes and alkenes. Yet, the *t*urn*o*ver *n*umber (TON) of *Ma*NifH (**Figure 4c**, *lower*), which is calculated based on the number of reduced carbons in products, is only 11% compared to that of *Ma*NifH (**Figure 4c**, *upper*).

The observation of differential reactivities of the all-ferrous *Ma*VnfH and *Ma*NifH proteins is important, as it highlights the crucial role of protein scaffolds in modulating the redox properties and catalytic capabilities of the active-site $[Fe_4S_4]$ centers of these proteins. More importantly, the fact that *Ma*VnfH can adopt the all-ferrous state at a reduction potential that is achievable under phys-

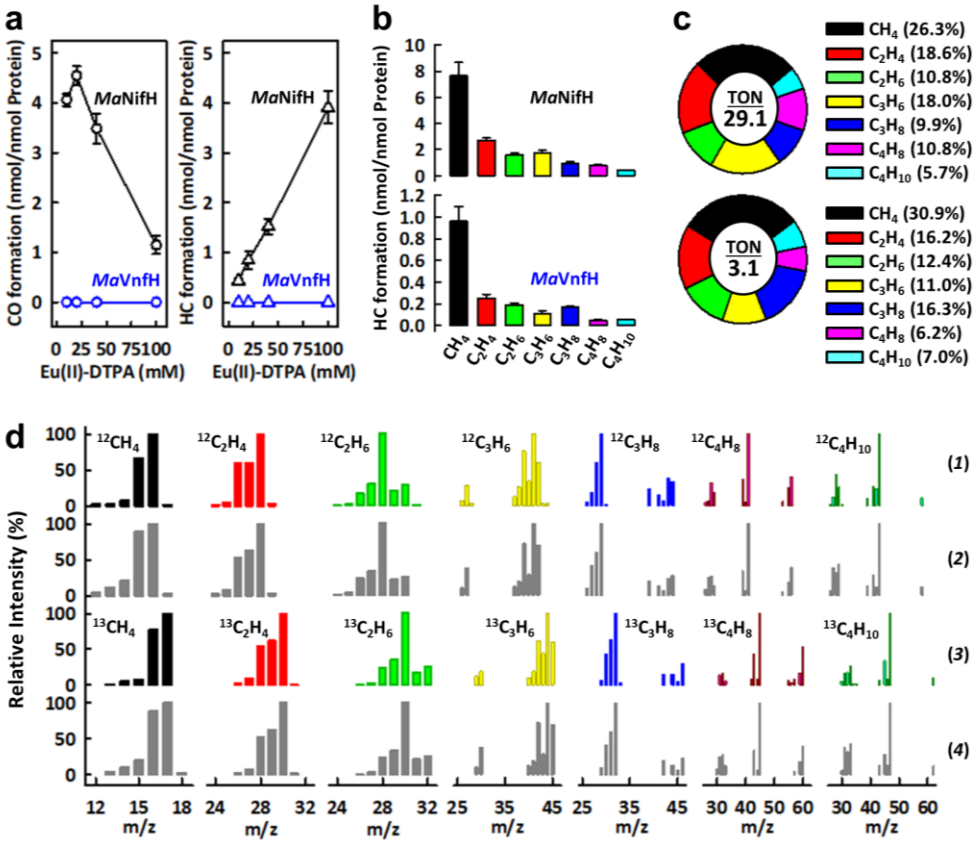

Figure 4. Reduction of CO_2 and CO by the all-ferrous *Ma*VnfH and *Ma*NifH proteins. (a) Yields of CO (*left*) and hydrocarbons (*right*) by *Ma*VnfH (*blue*) and *Ma*NifH (*black*) from CO_2 reduction at increasing Eu(II)-DTPA concentrations. Yields were calculated based on nmol of reduced C in CO or hydrocarbons per nmol protein. HC, hydrocarbons. (b) Identities and (c) distributions of hydrocarbons formed by *Ma*NifH (*upper*) and *Ma*VnfH (*lower*) from CO reduction at 100 mM Eu(II)-DTPA. TON, turnover number, was calculated based on the total nmol of reduced C in hydrocarbons generated per nmol protein. (d) GC-MS analysis of the hydrocarbon products generated from the reduction of ^{12}CO (*1*) or ^{13}CO (*3*) by *Ma*VnfH, shown in comparison with the fragmentation patterns of the corresponding ^{12}C-containing (*2*) or ^{13}C-labeled (*4*) hydrocarbon standards.

iological conditions[6,21-23] suggests the possibility that more Fe proteins may achieve and utilize this state for various cellular functions at similar or perhaps even more positive reduction potentials. This finding bears significant relevance to the long-standing debate in the field as to whether the Fe protein can only shuttle between the $[Fe_4S_4]^{1+}$ and $[Fe_4S_4]^{2+}$ states to support a one-electron transfer during catalysis or if it can also shuttle between the $[Fe_4S_4]^{0}$ and $[Fe_4S_4]^{2+}$ state to enable a two-electron electron transfer under physiological conditions.[24-26] The latter scenario is particularly important for nitrogenase catalysis, as it would cut the ATP consumption for electron transfer by half and thereby improve the energy economy of nitrogen fixation by twofold in the cell. The observation reported herein provides a useful platform for further investigation into the redox properties of the Fe protein, which is crucial for expanding our understanding of the reaction mechanism of the nitrogenase enzyme and the cellular energetics of the nitrogen-fixing microorganisms.

ASSOCIATED CONTENT

Supporting Information

The Supporting Information is available free of charge on the ACS Publications website.

Methods and additional experimental results as reported in Figures S1-S3 (PDF)

AUTHOR INFORMATION

Corresponding Author

*mribbe@uci.edu
*yilinh@uci.edu

Author Contributions

‖J.B.S., M.F.R. and C.J.H. contributed equally.

Notes

The authors declare no competing financial interests.

ACKNOWLEDGMENT

This work was supported by NSF Career grant CHE-1651398 (to Y.H.), which funded work related to the activity analysis and EPR characterization, and NSF grant CHE-1904131 (to M.W.R. and Y.H.), which funded work related to the titration experiments. The authors also wish to thank Prof. Jenny Y. Yang and Jeff M. Barlow (University of California, Irvine) for assistance with cyclic voltammetry experiments.

REFERENCES

(1) Burgess B. K.; Lowe, D. J. Mechanism of molybdenum nitrogenase. *Chem. Rev.* **1996**, *96*, 2983–3012.

(2) Schilter, D.; Camara, J. M.; Huynh, M. T.; Hammes-Schiffer, S.; Rauchfuss, T. B. Hydrogenase enzymes and their synthetic models: the role of metal hydrides. *Chem. Rev.* **2016**, *116*, 8693–8749.

(3) Mühlenhoff, U.; Hoffmann, B.; Richter, N.; Rietzschel, N.; Spantgar, F.; Stehling, O.; Uzarska, M. A.; Lill, R. Compartmentalization of iron between mitochondria and the cytosol and its regulation. *Eur. J. Cell. Biol.* **2015**, *94*, 292–308.

(4) O'Brien, E.; Holt, M. E.; Thompson, M. K.; Salay, L. E.; Ehlinger, A. C.; Chazin, W. J.; Barton, J. K. The [4Fe4S] cluster of human DNA primase functions as a redox switch using DNA charge transport. *Science* **2017**, *355*: eaag1789.

(5) Mettert, E. L.; Kiley, P. J. Fe-S proteins that regulate gene expression. *Biochim. Biophys. Acta.* **2015**, *1853*, 1284–1293.

(6) Rutledge, H. L.; Tezcan, F. A. Electron transfer in nitrogenase. *Chem. Rev.* **2020**, *120*, 5158–5193.

(7) Jasniewski, A. J.; Lee, C. C.; Ribbe, M. W.; Hu, Y. Reactivity, mechanism, and assembly of the alternative nitrogenases. *Chem. Rev.* **2020**, *120*, 5107–5157.

(8) Buscagan, T. M.; Rees, D. C. Rethinking the nitrogenase mechanism: activating the active site. *Joule* **2019**, *3*, 2662–2678.

(9) Lee, C. C.; Stiebritz, M. T.; Hu, Y. Reactivity of $[Fe_4S_4]$ clusters toward C1 substrates: mechanism, implications, and potential applications. *Acc. Chem. Res.* **2019**, 52, 1168–1176.

(10) Rebelein, J. G.; Stiebritz, M. T.; Lee, C. C.; Hu, Y. Activation and reduction of carbon dioxide by nitrogenase iron proteins. *Nat. Chem. Biol.* **2017**, *13*, 147–149.

(11) Stiebritz, M. T.; Hiller, C. J.; Sickerman, N. S.; Lee, C. C.; Tanifuji, K.; Ohki, Y.; Hu, Y. Ambient conversion of CO_2 to hydrocarbons by biogenic and synthetic $[Fe_4S_4]$ clusters. *Nat. Catal.* **2018**, *1*, 444–451.

(12) Rofer-DePoorter, C. K. A comprehensive mechanism for the Fischer-Tropsch synthesis. *Chem. Rev.* **1981**, *81*, 447–474.

(13) Angove, H. C.; Yoo, S. J.; Münck, E.; Burgess, B. K. An all-ferrous state of the Fe protein of nitrogenase. Interaction with nucleotides and electron transfer to the MoFe protein. *J. Biol. Chem.* **1998**, *273*, 26330–26337.

(14) Leggate, E. J.; Bill, E.; Essigke, T.; Ullmann, G. M.; Hirst, J. Formation and characterization of an all-ferrous Rieske cluster and stabilization of the $[2Fe\text{-}2S]^0$ core by protonation. *Proc. Natl. Acad. Sci. USA* **2004**, *101*, 10913–10918.

(15) Vincent, K. A.; Tilley, G. J.; Quammie, N. C.; Streeter, I.; Burgess, B. K.; Cheesman, M. R.; Armstrong, F. A. Instantaneous, stoichiometric generation of powerfully reducing states of protein active sites using Eu(II) and polyaminocarboxylate ligands. *Chem. Commun. (Camb)* **2003**, *20*, 2590–2591.

(16) Mayhew, S. G. The redox potential of dithionite and SO_2^- from equilibrium reactions with flavodoxins, methyl viologen and hydrogen plus hydrogenase. *Eur. J. Biochem.* **1978**, *85*, 535–547.

(17) Yoshizawa, J. M.; Blank, M. A.; Fay, A. W.; Lee, C. C.; Wiig, J. A.; Hu, Y.; Hodgson, K. O.; Hedman, B.; Ribbe, M. W. Optimization of FeMoco maturation on NifEN. *J. Am. Chem. Soc.* **2009**, *131*, 9321–9325.

(18) Yoo, S. J.; Angove, H. C.; Burgess, B. K.; Hendrich, M. P.; Münck, E. Mössbauer and integer-spin EPR studies and spin-coupling analysis of the $[4Fe\text{-}4S]^0$ cluster of the Fe protein from *Azotobacter vinelandii* nitrogenase. *J. Am. Chem. Soc.* **1999**, *121*, 2534–2545.

(19) Hiller, C. J.; Stiebritz, M. T.; Lee, C. C.; Liedtke, J.; Hu, Y. Tuning electron flux through nitrogenase with methanogen iron protein homologues. *Chemistry* **2017**, *23*, 16152–16156.

(20) Guo, M.; Sulc, F.; Ribbe, M. W.; Farmer, P. J.; Burgess, B. K. Direct assessment of the reduction potential of the $[4Fe\text{-}4S]^{(1+/0)}$ couple of the Fe protein from *Azotobacter vinelandii*. *J. Am. Chem. Soc.* **2002**, *124*, 12100–12101.

(21) Hosseinzadeh, P.; Lu, Y. Design and fine-tuning redox potentials of metalloproteins involved in electron transfer in bioenergetics. *Biochim. Biophys. Acta.* **2016**, *1857*, 557–581.

(22) Liu, J.; Chakraborty, S.; Hosseinzadeh, P.; Yu, Y.; Tian, S.; Petrik, I.; Bhagi, A.; Lu, Y. Metalloproteins containing cytochrome, iron-sulfur, or copper redox centers. *Chem. Rev.* **2014**, *114*, 4366–4469.

(23) Gao-Sheridan, H. S.; Pershad, H. R.; Armstrong, F. A.; Burgess, B. K. Discovery of a novel ferredoxin from *Azotobacter vinelandii* containing two [4Fe-4S] clusters with widely differing and very negative reduction potentials. *J. Biol. Chem.* **1998**, *273*, 5514–5519.

(24) Howard, J. B.; Rees, D. C. How many metals does it take to fix N_2? A mechanistic overview of biological nitrogen fixation. *Proc. Natl. Acad. Sci. USA* **2006**, *103*, 17088–17093.

(25) Erickson, J. A.; Nyborg, A. C.; Johnson, J. L.; Truscott, S. M.; Gunn, A.; Nordmeyer, F. R.; Watt, G. D. Enhanced efficiency of ATP hydrolysis during nitrogenase catalysis utilizing reductants that form the all-ferrous redox state of the Fe protein. *Biochemistry* **1999**, *38*, 14279–14285.

(26) Lowery, T. J.; Wilson, P. E.; Zhang, B.; Bunker, J.; Harrison, R. G.; Nyborg, A. C.; Thiriot, D.; Watt, G. D. Flavodoxin hydroquinone reduces *Azotobacter vinelandii* Fe protein to the all-ferrous redox state with a S = 0 spin state. *Proc. Natl. Acad. Sci. USA* **2006**, *103*, 17131–17136.

Insert Table of Contents artwork here

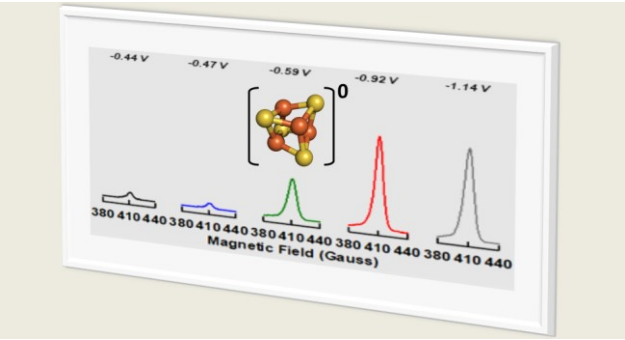

Supporting Information

Probing the all-ferrous states of methanogen nitrogenase iron proteins

Joseph B. Solomon,[†,‡,∥] Mahtab F. Rasekh,[†,‡,∥] Caleb J. Hiller,[§,∥] Chi Chung Lee,[†] Kazuki Tanifuji,[†] Markus W. Ribbe,[†,‡,*] Yilin Hu[†,*]

[†]Department of Molecular Biology and Biochemistry, University of California, Irvine, CA92697-3900

[‡]Department of Chemistry, University of California, Irvine, CA 92697-2025

[§]Department of Physical Science, Southern Utah University, Cedar City, UT 84720

*mribbe@uci.edu, yilinh@uci.edu

Methods

Cell Growth and Protein Purification. *E. coli* strains expressing His-tagged *Ma*NifH (strain YM135EE) and *Ma*VnfH (strain YM136EE)[1] were grown in 10-L batches in Difco LB medium containing 100 mg/L ampicillin (BD Biosciences) in a BIOFLO 415 fermenter (New Brunswick Scientific) at 37°C, with 200 rpm agitation and 10 L/min airflow. Growth rates were monitored by measuring cell density at 600 nm using a Spectronic 20 Genesys spectrometer (Spectronic Instruments). When OD_{600} reached 0.5, the temperature was lowered to 25°C before expression of *Ma*NifH or *Ma*VnfH was induced by addition of 25 μM IPTG. The *Ma*NifH or *Ma*VnfH protein was allowed to express for 16 h before cells were harvested by centrifugation using a Thermo Fisher Scientific Legend XTR centrifuge. Subsequently, His-tagged *Ma*NifH or *Ma*VnfH was purified by immobilized metal affinity chromatography (IMAC) using methods adapted from the purification of His-tagged nitrogenase proteins.[2,3] Specifically, 80 g of cell paste was resuspended in a buffer containing 25 mM Tris-HCl (pH 8.0), 2 mM sodium dithionite, 1 mM phenylmethylsulfonyl fluoride (PMSF) and 500 mM NaCl. The cell suspension was disrupted by a microfluidizer and centrifuged at 15,000 ×g to remove cell debris. The resultant, clear supernatant was loaded on a column packed with Ni sepharose 6 Fast Flow resin (~15 mL, GE Healthcare). Subsequently, the column was washed with a buffer containing 25 mM Tris-HCl (pH 8.0), 2 mM sodium dithionite, 500 mM NaCl and 40 mM imidazole, followed by elution of protein from the column with the same buffer containing 250 mM imidazole. The *Ma*NifH and *Ma*VnfH proteins were collected as dark brown eluents and subjected to further characterization (see below).

EPR Analysis. The electron paramagnetic resonance (EPR) samples were prepared in a Vacuum Atmospheres glove box with less than 5 ppm O_2 and flash frozen in liquid nitrogen prior to analysis. The dithionite-reduced samples contained 10 mg/mL of *Ma*NifH or *Ma*VnfH, 25 mM Tris-HCl (pH 8.0), 10% (vol/vol) glycerol, 250 mM imidazole, and 2 mM or 20 mM sodium dithionite. The europium(II) compound-reduced samples were prepared by incubating the sample with 10 mM europium(II) 1,4,7,10-tetrakis(carbamoylmethyl)-1,4,7,10-tetraazacyclododecane [Eu(II)-DOTAM], 10 mM europium(II) 1,4,7,10-tetraazacyclododecane-1,4,7,10-tetraacetic acid [Eu(II)-DOTA), or 10 mM europium(II) diethylenetriaminepentaacetic acid [Eu(II)-DTPA] for 5 min, followed by removal of excess Eu(II) compound using a G25 desalting column. EPR spectra were recorded by an ESP 300 E_z spectrophotometer (Bruker) interfaced with an ESR-9002 liquid-helium continuous-flow cryostat (Oxford Instruments) using a microwave power of 50 mW, a gain of 5×10^4, a modulation frequency of 100 kHz, and a modulation amplitude of 5 G. Five scans were recorded for each EPR sample at a temperature of 10 K and a microwave frequency of 9.62 GHz.

Determination of Reduction Potentials of Eu(II)-DOTA and Eu(II)-DOTAM. The cyclic voltammetry measurements of Eu(II)-DOTAM and Eu(II)-DOTA were performed on a Pine Wavedriver 10 potentiostat with AfterMath software in a glove box filled with dinitrogen. The conditions used to measure the samples were as follows: sample concentration, 1 mM; solvent, 25 mM Tris-HCl buffer (pH 8.0); temperature, room temperature; working electrode, vitreous carbon disc (1-mm diameter); auxiliary electrode, vitreous carbon rod; reference electrode, saturated calomel electrode (SCE, CH Instruments); supporting electrolyte, 200 mM KCl; sweep speed, 0.1 V/sec. The solution samples were prepared by diluting the bright yellow solutions of Eu(II)-DOTA and Eu(II)-DOTAM at 100 mM to the final concentration of 1 mM in the Tris-HCl buffer (pH 8.0) that contained 200 mM KCl. The potentials referenced to the SCE were converted to values with reference to the standard hydrogen electrode (SHE) by the following equation: E (*vs*. SHE) = E (*vs.* SCE) + 244 mV.[4]

CO_2- and CO-reduction assays. The *in vitro* CO_2- and CO-reduction assays were carried out in 9.4 mL assay vials with crimped butyl rubber serum stoppers. Each assay contained, in a total volume of 1.0 mL, 0.5 mg *Ma*NifH or *Ma*VnfH, increasing concentrations (10, 20, 40 or 100 mM; for CO_2-reduction assays) or 100 mM (for CO-reduction assays) of Eu(II)-DTPA, and either 500 mM Tris-HCl, pH 10 (for CO_2-reduction assays) or 250 mM Tris-HCl, pH 8 (for CO-reduction assays). The CO-reduction assays of *Ma*VnfH were conducted in the presence of ^{12}CO or ^{13}CO. The optimum concentration of CO_2 (100%) or CO (0.53%), which resulted in the maximum amount of product(s), was determined by titration with increasing concentrations of CO_2 or CO added to the headspace of the respective assay. The CO_2-reduction assays were assembled by repeatedly flushing and exchanging the buffer solution without Eu(II)-DTPA and protein with 100% CO_2, followed by equilibration for 30 min until pH stabilized at ~8.1; whereas the CO-reduction assays were assembled by repeatedly flushing and exchanging the buffer solution without Eu(II)-DTPA and protein with 100% Ar, followed by addition of 0.53% CO. The reaction was initiated by addition of *Ma*NifH or *Ma*VnfH, followed by immediate addition of Eu(II)-DTPA. The assay mixture was then incubated with continuous shaking at 30°C until the reaction was complete (300 min), followed by quenching with 100 µL of 30% trichloroacetic acid. The headspace sample was subsequently examined for CO- and hydrocarbon-formation as described earlier.[5]

GC-MS analysis. The products of ^{12}CO- and ^{13}CO-reduction by *Ma*VnfH were analyzed by gas chromatography-mass spectrometry (GC-MS) using a Thermo Scientific Trace 1300 GC system coupled to a Thermo ISQ QD (Thermo Electron North America LLC). Specifically, a total of 250 µL headspace sample was injected into a split/splitless injector operated at 150°C in split mode with a split ratio of 10, followed

by separation of gas on a HP-PLOT/Q+PT column (30 m × 0.32 mm ID × 20 μm film; Agilent Technologies North America LLC), which was held at 30°C for 3 min, heated to 200°C at a rate of 15°C/min, and held at 200°C for 5 min. The rate at which the carrier helium (He) gas passed through the column was held at 0.7 mL/min for 4 min, increased to 1.4 mL/min at a rate of 0.5 mL/min, and held at 1.4 mL/min for the remainder of the run. The mass spectrometer was operated in the electron impact (EI) ionization mode. The fragmentation patterns of the products were compared to those of the C_1-C_4 alkane and alkene standards as described previously.[5]

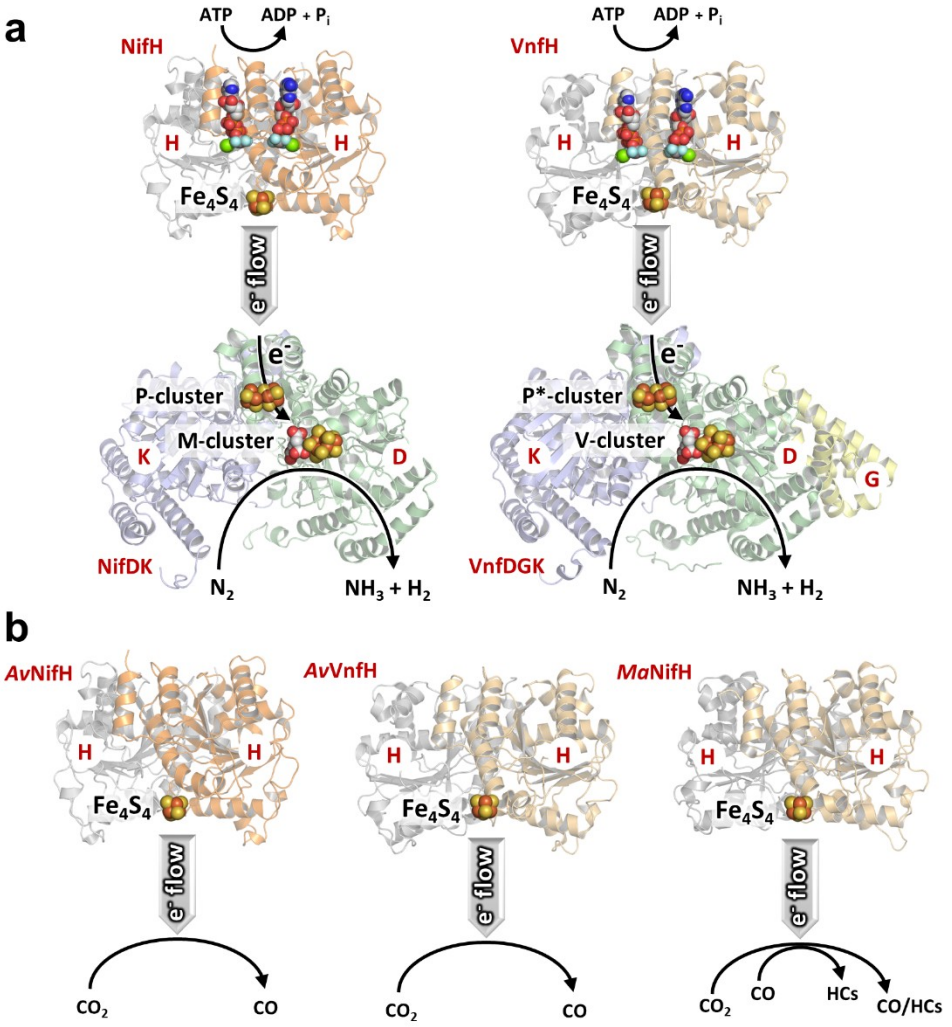

Figure S1. Functions of Fe protein (a) as an electron donor to its catalytic partner to enable nitrogenase catalysis or (b) as an independent reductase of C1 substrates. (a) Catalysis by the Mo- (left) or V- (right) nitrogenase, which involves transfer of electrons from the [Fe_4S_4] cluster of the Fe protein (NifH or VnfH), via the P- or P*-cluster, to the M- or V-cluster of the catalytic partner (NifDK or VnfDGK), where substrate reduction takes place. (b) Catalysis by the nucleotide-free NifH or VnfH as an independent reductase of C1 substrates. The NifH (left) and VnfH (right) proteins from *Azotobacter vinelandii* (designated *Av*NifH and *Av*VnfH, respectively) can reduce CO_2 to CO; whereas the NifH protein from *Methanosarcina acetivorans* (designated *Ma*NifH) can reduce CO_2 and CO to hydrocarbons. The subunits of the Fe proteins are colored yellow and orange, the subunits of the catalytic partners are colored light green, light blue, and yellow. Atoms are colored as follows: Fe, orange; S, yellow; C, gray; Mo, teal; V, dark gray; O, red; N, blue; P, tangerine; Mg, green; Al, light blue. PDB entries 1N2C,[6] 5N6Y,[7] 6Q93,[8] and 6NZJ[9] were used to generate this figure.

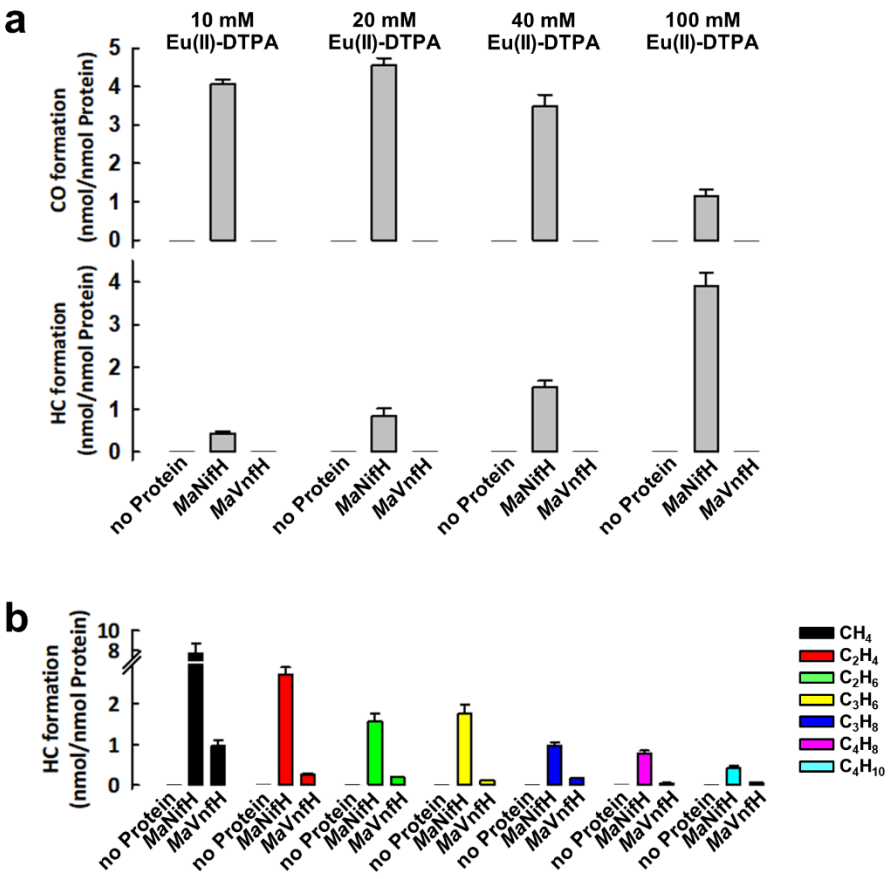

Figure S2. *Ma*NifH- and *Ma*VnfH-dependent reduction of CO_2 and CO in the presence of Eu(II)-DTPA. (a) Formation of CO (upper) and hydrocarbons (lower) by *Ma*VnfH and *Ma*NifH from CO_2 reduction at various Eu(II)-DTPA concentrations. (b) Formation of hydrocarbons by *Ma*NifH and *Ma*VnfH from CO reduction at 100 mM Eu(II)-DTPA. Yields were calculated based on nmol of reduced C in CO or hydrocarbons per nmol protein. No products were detected in the absence of *Ma*VnfH or *Ma*NifH. HC, hydrocarbons

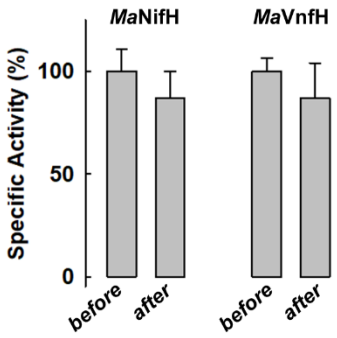

Figure S3. Specific activities of *Ma*NifH and *Ma*VnfH before and after the CO_2 reduction assay conducted in the presence of 100 mM Eu(II)-DTPA. The proteins were assayed with NifDK from *Azotobacter vinelandii* as described earlier.[1] Both Fe proteins remained mostly active at the end of the CO_2 reduction assays, suggesting that the [Fe_4S_4] clusters in these proteins were mostly intact after the reaction. The specific activities of *Ma*NifH (91 $\pm$ 10 nmol C_2H_4/mg protein/min) and *Ma*VnfH (187 $\pm$ 12 nmol C_2H_4/mg protein/min) before the CO_2 reduction assays were set as 100%, and the % specific activities of these Fe proteins after the CO_2 reduction assays were calculated accordingly.

References

(1) Hiller, C. J.; Stiebritz, M. T.; Lee, C. C.; Liedtke, J.; Hu, Y. Tuning electron flux through nitrogenase with methanogen iron protein homologues. *Chemistry* **2017**, *23*, 16152-16156.

(2) Ribbe, M. W.; Hu, Y.; Guo, M.; Schmid, B.; Burgess, B. K. The FeMoco-deficient MoFe protein produced by a *nifH* deletion strain of *Azotobacter vinelandii* shows unusual P-cluster features. *J. Biol. Chem.* **2002**, *277*, 23469-23476.

(3) Burgess, B. K.; Jacobs, D. B.; Stiefel, E. I. Large-scale purification of high activity *Azotobacter vinelandii* nitrogenase. *Biochim. Biophys. Acta.* **1980**, *614*, 196-209.

(4) Sawyer, D. T.; Sobkowiak, A.; Roberts, J. L. Electrochemistry for Chemists, 2nd Edition. Wiley, New York, NY, **1995**.

(5) Stiebritz, M. T.; Hiller, C. J.; Sickerman, N. S.; Lee, C. C.; Tanifuji, K.; Ohki, Y.; Hu, Y. Ambient conversion of CO_2 to hydrocarbons by biogenic and synthetic [Fe_4S_4] clusters. *Nat. Catal.* **2018**, *1*, 444-451.

(6) Schindelin H, Kisker C, Schlessman JL, Howard JB & Rees DC. Structure of ADP x AlF_4^--stabilized nitrogenase complex and its implications for signal transduction. *Nature* **1997**, *387*, 370-376.

(7) Sippel D & Einsle O. The structure of vanadium nitrogenase reveals an unusual bridging ligand. *Nat. Chem. Biol.* **2017**, *13*, 956-960.

(8) Rohde M, Trncik C, Sippel D, Gerhardt S & Einsle O. Crystal structure of VnfH, the iron protein component of vanadium nitrogenase. *J. Biol. Inorg. Chem.* **2018**, *23*, 1049-1056.

(9) Rettberg LA, Kang W, Stiebritz MT, Hiller CJ, Lee CC, Liedtke J, Ribbe MW & Hu Y. Structural analysis of a nitrogenase iron protein from *Methanosarcina acetivorans*: Implications for CO_2 capture by a surface-exposed [Fe_4S_4] cluster. *mBio* **2019**, *10*, e01497-19.